A Factor Set Based GNSS Fault Detection and Exclusion for Vehicle Navigation in Urban Environments

Hanzhi Chen
Nanjing University of Aeronautics and Astronautics
Rui Sun (rui.sun@nuaa.edu.cn)
Nanjing University of Aeronautics and Astronautics
Qi Cheng
Hong Kong Polytechnic University
Lei Yang
Nanjing University of Aeronautics and Astronautics

Research Article

Keywords: GNSS, IMU, integrated navigation, urban positioning, fault detection and exclusion

Posted Date: July 26th, 2022

DOI: https://doi.org/10.21203/rs.3.rs-1865103/v1

A Factor Set Based GNSS Fault Detection and Exclusion for Vehicle Navigation in Urban Environments

Hanzhi Chen[a,b], Rui Sun[a*], Qi Cheng[c], Lei Yang[a]

[a]College of Civil Aviation, Nanjing University of Aeronautics and Astronautics, Nanjing 211106, China

[b]State Key Laboratory of Air Traffic Management System and Technology, Nanjing 210007, China

[c]the Dept. of Land Surveying and Geo-Information, Hong Kong Polytechnic University, Hongkong, China

rui.sun@nuaa.edu.cn

Abstract

With the rapid development of safety critical applications of Intelligent Transportation Systems (ITS), Global Navigation Satellite System (GNSS) fault detection and exclusion (FDE) methods have made navigation systems increasingly reliable. However, in multi-fault scenarios of urban environments, FDE methods generally demand massive calculations and have a high risk of missed detection and false alarm. To deal with this issue, we proposed a factor set based FDE algorithm for the integration of GNSS and Inertial Measurement Units (IMU). The FDE is first performed efficiently via consistency checking over far fewer subsets of the pseudorange. Afterwards, the FDE results are validated by missed-detection and false-alarm checks. The missed-detection-check factor is designed by predicting the maximum horizontal GNSS positioning error, while the false-alarm-check factor is designed with the aid of IMU mechanization. Following FDE, a loosely coupled GNSS/IMU integration is carried out to output the final estimation of the position, velocity and attitude of the vehicle. The proposed algorithm improved both horizontal and 3D positioning accuracy by more than 50% in the field test, compared to the traditional GNSS/IMU loosely coupled scheme. Additionally, with the proposed algorithm, the resultant accuracy of the velocity and of the heading angle were improved by over 20% and 50% respectively.

Keywords: GNSS, IMU, integrated navigation, urban positioning, fault detection and exclusion

Introduction

For decades, the fusion of Global Navigation Satellite Systems (GNSS) and Inertial Measurement Units (IMU) has been of essential importance in its applications toward vehicular navigation (Sun et al. 2010; Chen et al. 2020). With the development of safety critical applications of Intelligent Transportation Systems (ITS), the necessity for navigation systems to be reliable has become more and more stringent (Feng and Ochieng 2007; Wang et al. 2020). However, it should be noted that GNSS pseudoranges may contain gross errors due to multipath interferences and non-line-of-sight (NLOS) receptions in urban environments (Macgougan et al. 2002; Sun et al. 2022). Faulty GNSS measurements significantly reduce the reliability of vehicular navigation systems in urban environments, with the driver's life becoming threatened in the worst cases (Cheng et al. 2021). Therefore, it is of urgent necessity and importance to develop an efficient algorithm to detect and exclude faulty GNSS measurements to enhance the navigation safety.

Fault detection and exclusion (FDE) methods typically work by checking the consistency of GNSS measurements (Sabatini et al. 2017; Li et al. 2020). Generally, FDE methods can be classified into two categories: snapshot FDE and recursive FDE (Zabalegui et al. 2020). Snapshot FDE only checks the consistency of current measurements, while recursive FDE utilises both current and previously recorded historical measurements. Originally, FDE was applied in civil aviation as a major part of Receiver Autonomous Integrity Monitoring (RAIM) (Feng et al. 2006; Wang and Ober 2009). In the 1980s, classical FDE algorithms, including the pseudorange comparison method (Lee 1986), the least square residual (LSR) method (Parkinson and Axelrad 1988) and the parity vector method (Sturza 1988), were proposed successively. These three classical FDE algorithms are all based on single-fault assumptions. With the development of multi-frequency and multi-constellation GNSS, more satellites and signals are available: this does, however, mean that, the risk of multiple faults gets higher and cannot be ignored at the same time. Consequently, Advanced RAIM (ARAIM) was proposed based on multiple-hypothesis solution separation (Blanch et al. 2012, 2013). In theory, ARAIM is able to detect multiple faults, but as a large number of subsets are involved in consistency checks, the consumption of computational resources is very high. Notably, the FDE schemes of classic RAIM and ARAIM are all snapshot. Alternatively, recursive Kalman Filter (KF) based FDE were also developed (Bhattacharyya and Mute 2020), however, may fail due to undetected faults in historical epochs.

To improve the reliability of vehicular navigation systems, applying FDE to land transportation, on top of civil aviation, has also been proposed. There are, however, limitations when doing so, as FDE designed specifically for civil aviation cannot be implemented directly into urban environments, where measurement redundancy is low and the possibility of simultaneous multiple faults is much higher (Zhu et al. 2018).

Information space projection-based methods (Kaddour et al. 2015) and recursive consistency check-based FDE (Blanch et al. 2015) have been proposed to deal with multi-fault scenarios. These methods, however, demand a large amount of computing resources to enact, and have only been verified by simulated data. FDE based on innovation of GNSS/IMU fusion have also been applied to improve the performance of integrated navigation systems (Hwang et al. 2005; Zhu et al. 2017; Sun et al. 2021). Though these innovation-based FDE methods are valid for multiple faults and avoid numerous subsets based consistency check, it should be noted that errors in IMU measurements could result in potentially false FDE. In addition, the difficulty of detecting and excluding simultaneous multiple faults also increases the risk of false alarm and missed detection greatly. However, for GNSS FDE applied in integrated navigation, most of the research directly inputs the FDE results to the filter of integration, which significantly reduces the robustness of the navigation system.

As demonstrated above, current FDE methods are not well suited to combat performance degradation of vehicle navigation in urban areas, due to current FDE methods demanding large amounts of calculations, as well as having high risk of false alarm and missed detection. To overcome this problem, we proposed a new factor set based FDE algorithm. In particular, simultaneous multiple faults can be detected and iteratively excluded by consistency checking over the universal set and single-fault hypothesis subsets of the pseudoranges with fewer computational resources required. Also, the improvement of the correctness and robustness of FDE is achieved by reducing the possibility of missed detection and false alarm. The missed-detection check is performed by predicting the maximum of horizontal GNSS positioning error, while the false-alarm check is based on the vehicular position reckoned by IMU mechanization.

Algorithm framework

The framework of the proposed algorithm is shown in Fig. 1. In this figure, N_B and N_G are current number of BDS and GPS satellites, which could be reduced due to fault exclusion. In addition, F_{LS} and F_{update} are two constants used in the judgement segments of the algorithm. On the whole, the proposed FDE scheme has two steps, preliminary FDE and FDE validation. Specifically, in step one, when $N_B \geq 4$ and $N_G \geq 4$, the fault-detection factor $S_{k,0}^{LS}$ is calculated and compared with the predetermined threshold T^{LS}. If $S_{k,0}^{LS} \leq T^{LS}$, F_{LS} is set to 1. Otherwise, iterative fault exclusion is implemented as follows. In the first iteration of fault exclusion, the single-fault-hypothesis subsets of the pseudorange are constructed to obtain the minimum fault-exclusion factor $(S_{k,j}^{LS})_{min}$. And the measurement excluded by the subset corresponding to $(S_{k,j}^{LS})_{min}$ is marked as faulty. Then, if $(S_{k,j}^{LS})_{min} > T^{LS}$, the fault-exclusion iteration needs to be continued until all faults have been excluded or the condition $N_B + N_G > 6$, $N_B \geq 1$ and $N_G \geq 1$ is not satisfied.

In step two of the proposed FDE scheme, missed-detection check or false-alarm check is performed. When $F_{LS} = 1$, missed-detection-check factor S_k^{MD} is calculated and compared with the threshold T^{MD}. If $S_k^{MD} \leq T^{MD}$, the variances of pseudorange residuals are updated and F_{update} is set to 1. Otherwise, F_{update} is set to 0. When $F_{LS} = 0$, false-alarm-check factor S_k^{FA} is calculated and compared with the threshold T^{FA} to determine the value of F_{update}.

Above is the basic procedure of the proposed FDE. After the two-step FDE, if $F_{update} = 1$, the vehicular navigation state reckoned by IMU mechanization gets updated by the solution of remained GNSS measurements to obtain the final estimations of vehicular position, velocity and altitude.

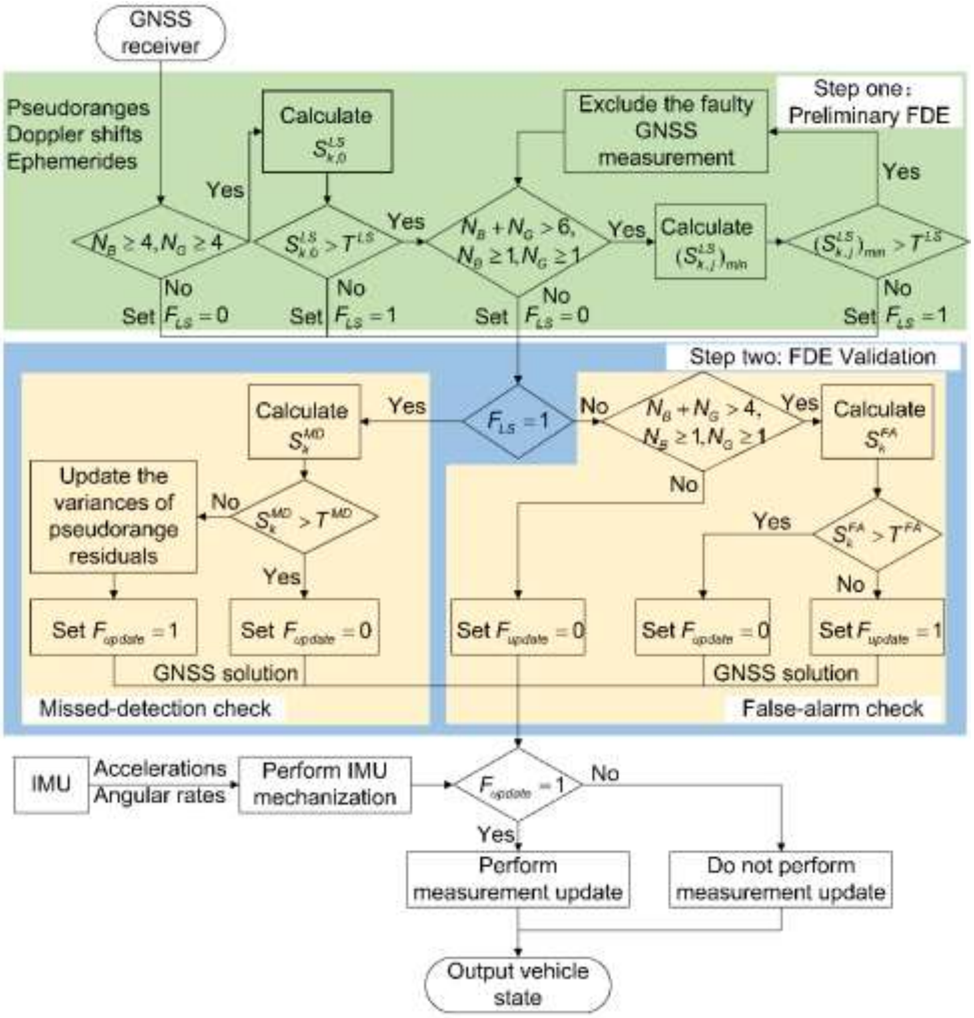

Fig. 1 Framework of the proposed algorithm

Preliminary FDE

In step one, preliminary FDE is performed and the flag F_{LS} used in step two is determined. If $N_B \geq 4$ and $N_G \geq 4$, the LSR solution of the position is calculated with all the pseudoranges whose ionosphere delays, troposphere delays and satellite clock errors have been corrected with corresponding models. Then, the fault-detection factor is defined as:

$$S_{k,0}^{LS} = \sqrt{\sum_{i=1}^{N_B+N_G} \frac{r_i^2}{\sigma_i^2}} \tag{2.1}$$

where r_i is the ith element of the pseudorange residual vector $\boldsymbol{r}$; σ_i is the standard deviation of the pseudorange residual of satellite i. The value of σ_i is determined with experience initially and updated by the formula (2.14) in the following epochs.

It is assumed that the pseudoranges are only affected by nominal errors which obey zero-mean Gaussian distributions in fault-free cases, while one or more pseudoranges contain a large bias in faulty cases. Under this assumption, we can obtain that:

$$\text{In fault-free cases, } (S_{k,0}^{LS})^2 \sim \chi^2(m, 0) \tag{2.2}$$

$$\text{In faulty cases, } (S_{k,0}^{LS})^2 \sim \chi^2(m, \lambda),\ \lambda \neq 0 \tag{2.3}$$

where $\chi^2(m, 0)$ represents central Chi square distribution with m degrees of freedom; m equals $N_B + N_G - 5$; $\chi^2(m, \lambda)$ represents non-central Chi square distribution with m degrees of freedom and the non-centrality parameter λ.

The threshold of $S_{k,0}^{LS}$ is obtained by

$$T^{LS} = \sqrt{F_{\chi^2(m,0)}^{-1}(1 - P_{FA})} \tag{2.4}$$

where $F_{\chi^2(m,0)}^{-1}$ is the inverse of the cumulative probability distribution function of $\chi^2(m, 0)$; P_{FA} is the predetermined false-alarm probability.

If $S_{k,0}^{LS} < T^{LS}$, all pseudoranges are marked as normal measurements, and F_{LS} is set to 1. Otherwise, faulty measurements are believed to exist, and fault exclusion should be performed. Firstly, all single-fault-hypothesis subsets which exclude one pseudorange and include at least one BDS pseudorange and one GPS pseudorange are constructed:

$$A_{k,1}, A_{k,2}, \cdots, A_{k,N_A^1} \tag{2.5}$$

where $A_{k,i}$ $(i = 1,2,\cdots,N_A^1)$ represents the i th single-fault-hypothesis subset;

subscripts k and i mean indexes of the epoch and the subsets, respectively; N_A^1 is the number of subsets in the first iteration.

Based on those subsets, we can obtain the test statistics of each subset according to formula (2.1):

$$S_{k,1}^{LS}, S_{k,1}^{LS}, \cdots, S_{k,N_A^1}^{LS} \tag{2.6}$$

Their thresholds can be calculated according to formula (2.4), but it should be pointed out that the degrees of freedom should be reduced by one.

If the minimum test statistics, $(S_{k,j}^{LS})_{min}$, is lower than the threshold T^{LS}, the pseudorange excluded by the subset corresponding to $(S_{k,j}^{LS})_{min}$ is regarded as a faulty measurement, and F_{LS} is set to 1. Otherwise, the next fault-exclusion iteration is performed on the subset corresponding to $(S_{k,j}^{LS})_{min}$. And the iteration is continued until all faults have been excluded or $N_B + N_G > 6$, $N_B \geq 1$ and $N_G \geq 1$ is not satisfied (single-fault-hypothesis subsets with redundancy can't be constructed appropriately under this condition).

Missed-detection check

If F_{LS} is equal to 1, all the remaining pseudoranges are marked as normal measurements by preliminary FDE. However, it is possible that faulty measurements still exist. Hence, to reduce the risk of missed detection, the theoretical undetected maximum of the horizontal positioning errors of the GNSS solution is predicted. The theoretical maximum of vertical or 3D positioning errors is not used in the missed-detection check after the attempt in the field test. With the predetermined possibility of missed detection, P_{MD}, the maximum undetectable non-centrality parameter, $\lambda_{\max}$, can be obtained by solving:

$$P_{MD} = \int_0^{(T_{final}^{LS})^2} f_{\chi^2(m_{final},\lambda_{max})}(x)dx \tag{2.7}$$

where T_{final}^{LS} and m_{final} represent the threshold and degrees of freedom of Chi square distribution corresponding to the set of the finally remaining pseudorange, respectively.

Matrix $\boldsymbol{H}^+$ is the pseudo inverse of the GNSS observation matrix $\boldsymbol{H}$:

$$\boldsymbol{H}^+ = (\boldsymbol{H}^T\boldsymbol{H})^{-1}\boldsymbol{H}^T \tag{2.8}$$

Matrix $\boldsymbol{S}$ can be obtained by:

$$\boldsymbol{S} = \boldsymbol{I} - \boldsymbol{H}\boldsymbol{H}^+ \tag{2.9}$$

where $\boldsymbol{I}$ is an identity matrix whose size is the same as that of matrix $\boldsymbol{H}\boldsymbol{H}^+$.

The $k_{slope,i}$, which projects the pseudorange error of satellite i onto horizontal positioning domain, can be calculated by：

$$k_{slope,i} = \sqrt{\frac{(H_{1,i}^+)^2 + (H_{2,i}^+)^2}{S_{i,i}}} \tag{2.10}$$

where $H_{1,i}^+$ represents the element in the 1st row and ith column of the matrix $\boldsymbol{H}^+$; $H_{2,i}^+$ represents the element in the 2nd row and ith column of the matrix $\boldsymbol{H}^+$; $S_{i,i}$ is the ith diagonal element of the matrix $\boldsymbol{S}$.

Then, the predicted maximum of the horizontal GNSS positioning error was defined as the missed-detection-check factor:

$$S_k^{MD} = \{\sigma_i \cdot k_{slope,i}\}_{max} \cdot \sqrt{\lambda_{min}} \tag{2.11}$$

The threshold of S_k^{MD} is obtained by:

$$T^{MD} = \mu_{MD} + \alpha \cdot \sigma_{MD} \tag{2.12}$$

where μ_{MD} is the mean of S_k^{MD}; σ_{MD} is the standard deviation of S_k^{MD}; α is an empirical coefficient taking a value from 3 to 5.

The variances of pseudorange residuals are initialized at the first epoch. In the later epochs, they get updated by the data in the sliding window:

$$\begin{matrix} r_{1,k-L+1} & r_{1,k-L+2} & \cdots & null \\ null & r_{2,k-L+2} & \cdots & r_{2,k} \\ \vdots & \vdots & \ddots & \vdots \\ r_{C_B+C_G,k-L+1} & null & \cdots & r_{C_B+C_G,k} \end{matrix} \tag{2.13}$$

Where C_B and C_G are the numbers of satellites in BDS and GPS constellations, respectively; $r_{i,j}(i = 1,2,\cdots,C_B + C_G\ ;\ j = k - L + 1, k - L + 2,\cdots,k)$ is the pseudorange residual of satellite i at epoch j; L is the empirical length of the sliding window generally taking the value of 1000; $null$ means corresponding pseudorange residual is empty because the satellite is invisible, or the pseudorange is faulty in step one of the corresponding epoch.

The variance of the pseudorange residual of satellite i is updated by:

$$\sigma_i = \begin{cases} \sqrt{\frac{\sum_{j=1}^{N_i}(r_{i,j})^2}{N_i}}, & N_i > \beta L, \sqrt{\frac{\sum_{j=1}^{N_i}(r_{i,j})^2}{N_i}} > \sigma_i^{min} \\ \sigma_i^{min}, & N_i > \beta L, \sqrt{\frac{\sum_{j=1}^{N_i}(r_{i,j})^2}{N_i}} \le \sigma_i^{min} \\ \sigma_i^{pre}, & N_i \le \beta L \end{cases} \tag{2.14}$$

where N_i represents the count of non-empty pseudorange residuals of satellite i; β is the empirical coefficient taking the value between 0.7 and 0.9; σ_i^{min} is the predetermined minimum of σ_i; σ_i^{pre} is the standard deviation of pseudorange residual of satellite i in the last epoch.

False-alarm check

In the case when F_{LS} is equal to 0 after step one, either the visible satellites are too few for the proposed fault detection scheme, or the fault exclusion iteration cannot be performed or continued. If the GNSS data is to be abandoned directly in this case, measurement update would not be performed at this epoch. It increases the risk of error divergence of integrated navigation systems. Therefore, we proposed a false-alarm-check scheme as follows.

If the condition $N_B + N_G > 4$, $N_B \geq 1$ and $N_G \geq 1$ is not satisfied, F_{update} is set to 0. Otherwise, based on the GNSS position solution and the lever arm between GNSS antenna and IMU, the position of IMU can be estimated:

$$\boldsymbol{P}_k^{GNSS} = (p_X^{GNSS}, p_Y^{GNSS}, p_Z^{GNSS})^T \tag{2.15}$$

where p_X^{GNSS}, p_Y^{GNSS} and p_Z^{GNSS} are respectively estimated X, Y and Z coordinates of the IMU with GNSS pseudoranges in earth-centered earth-fixed frame (e frame).

At this epoch, the estimated position of the IMU can also be obtained by IMU mechanization:

$$\boldsymbol{P}_k^{IMU} = (p_X^{IMU}, p_Y^{IMU}, p_Z^{IMU})^T \tag{2.16}$$

where p_X^{IMU}, p_Y^{IMU} and p_Z^{IMU} are respectively the estimated X, Y and Z coordinates of the IMU in e frame by IMU mechanization.

Then, the innovation in position domain can be obtained as follows:

$$\boldsymbol{I}_k^{Pos} = \boldsymbol{P}_k^{GNSS} - \boldsymbol{P}_k^{IMU} \tag{2.17}$$

The false-alarm-check factor is defined as:

$$S_k^{FA} = \left|\boldsymbol{I}_k^{Pos}\right| \tag{2.18}$$

The threshold can be obtained by:

$$T^{FA} = \mu_{FA} + \gamma\sigma_{FA} \tag{2.19}$$

where μ_{FA} is the mean of S_k^{FA}; γ is an empirical coefficient which takes a value from 3 to 6; σ_{FA} is the standard deviation of S_k^{FA}.

If $S_k^{FA} > T^{FA}$, F_{update} is set to 0. Otherwise, the remaining GNSS measurements are remarked as normal measurements and F_{update} is set to 1.

GNSS/IMU Fusion Scheme

As the FDE is performed in the position domain, Extended Kalman Filter (EKF) based Loosely Coupled (LC) scheme is utilized to fuse GNSS and IMU. The state vector is defined as:

$$\boldsymbol{X}_k = \left[(\delta\boldsymbol{r}_{IMU}^{e})^T \quad (\delta\boldsymbol{v}_{IMU}^{e})^T \quad (\delta\boldsymbol{\phi}_{IMU}^{e})^T \quad (\boldsymbol{b}_g)^T \quad (\boldsymbol{b}_a)^T \quad (\boldsymbol{s}_g)^T \quad (\boldsymbol{s}_{\boldsymbol{a}})^T\right]^T \tag{2.20}$$

where $\delta\boldsymbol{r}_{IMU}^{e}$, $\delta\boldsymbol{v}_{IMU}^{e}$, $\delta\boldsymbol{\phi}_{IMU}^{e}$ are the position error vector, the velocity error vector and the attitude error vector of IMU mechanization in e-frame, respectively; $\boldsymbol{b}_g$ and $\boldsymbol{b}_a$ are the vectors of gyroscope and accelerometer three-axis biases, respectively; $\boldsymbol{s}_g$ and $\boldsymbol{s}_a$ are the vectors of gyroscope and accelerometer three-axis scale factors, respectively.

After FDE, if $F_{update} = 0$, the measurement update is not performed, otherwise the state vector is updated with the measurement vector:

$$\boldsymbol{Z}_k = \begin{bmatrix} p_X^{GNSS} - p_X^{IMU} \\ p_Y^{GNSS} - p_Y^{IMU} \\ p_Z^{GNSS} - p_Z^{IMU} \\ v_X^{GNSS} - v_X^{IMU} \\ v_Y^{GNSS} - v_Y^{IMU} \\ v_Z^{GNSS} - v_Z^{IMU} \end{bmatrix} \tag{2.21}$$

where $(v_X^{GNSS}, v_Y^{GNSS}, v_Z^{GNSS})$ is the velocity solution with GNSS Doppler shifts in the e-frame and the lever arm effect has been corrected; $(v_X^{IMU}, v_Y^{IMU}, v_Z^{IMU})$ is the estimated velocity by IMU mechanization in the e-frame.

Next, the estimated position, velocity and altitude get corrected utilizing the state vector of the EKF, thus, the final estimation of the vehicular state would be the output.

Field test and results analysis

A field test was conducted in order to validate the proposed algorithm on November 10, 2021, in Nanjing, China. The experimental vehicle and equipment are shown in Fig. 2. The raw GNSS data were collected with a BDStar Navigation C520-AT receiver at a sample rate of 10Hz, while the raw IMU data were collected with a MEMS IMU, STIM-300, at a sampling rate of 125Hz. The reference trajectory was determined by the post processing kinematic mode of the data from a high grade inertial/GNSS navigator, HGuide N580, and the data from a GNSS base station in Hohai University with NovAtel Inertial Explorer software. Antenna 1 and 2 are both ZYACF-S806 antennas of Zhejiang ZhongYu Communication Technology Co., Ltd. The HGuide N580 was connected with antenna 1, and the BDStar Navigation receiver was connected with antenna 2.

Fig. 2 Experimental setup

The vehicle was driven around the area near Nanjing South Railway Station. Fig. 3

shows the driving trajectory of our experimental vehicle in this test. In the four parts of the trajectory, the positioning errors of the traditional GNSS/IMU fusion algorithm are much bigger. Part 1 of the trajectory is situated around the start point because the vehicle was static during this period.

Fig. 3 The trajectory of our experimental vehicle in the test

The experimental scenes in the four parts of the trajectory are shown as Fig. 4. Tall buildings are situated on either side of part 1 and part 3 of the trajectory. The vehicle was driven through a tunnel in part 2 of the trajectory, and under elevated roads in part 4 of the trajectory.

Fig. 4 Partial experimental scenes

Table 1 shows the setting of relevant parameters of the proposed algorithm. Both P_{FA} and P_{MD} were set to 1×10^{-5} since we referred to the classical RAIM in civil aviation and adjusted them according to the results of the experiment. By analyzing historical data collected in the same area on another day, November 9, 2021, we calculated the mean and standard deviations of the missed-detection-check factor and false-alarm-check factor, resulting in our choice to set the thresholds T^{MD} and T^{FA} to 9 and 40 respectively.

Table 1 The values of relevant parameters of the proposed algorithm

Parameter	Value
The possibility of false alarm, P_{FA}	1×10^{-5}
The possibility of missed detection, P_{MD}	1×10^{-5}
The threshold of missed-detection-check factor, T^{MD}	9
The threshold of false-alarm-check factor, T^{FA}	40

As illustrated before, the preliminary FDE is performed first. Fig. 5 compares the fault-detection factor and its threshold at the start of step one. Since the scale of the vertical axis is too large for the threshold in the upper subfigure, the part in the yellow dashed rectangle is consequently enlarged, as seen in the lower subfigure. From Fig. 5, it can be seen that the fault-detection factor exceeds the threshold a large part of the time, about 75% percent of the time specifically. Additionally, the value of the fault-detection factor exceeds 100 in many epochs, and exceeds 1000 in a few epochs, while the threshold remains at 7 approximately. These characteristics of Fig. 5 are due to the complex environment of the experimental area, where GNSS measurements easily arise as faulty.

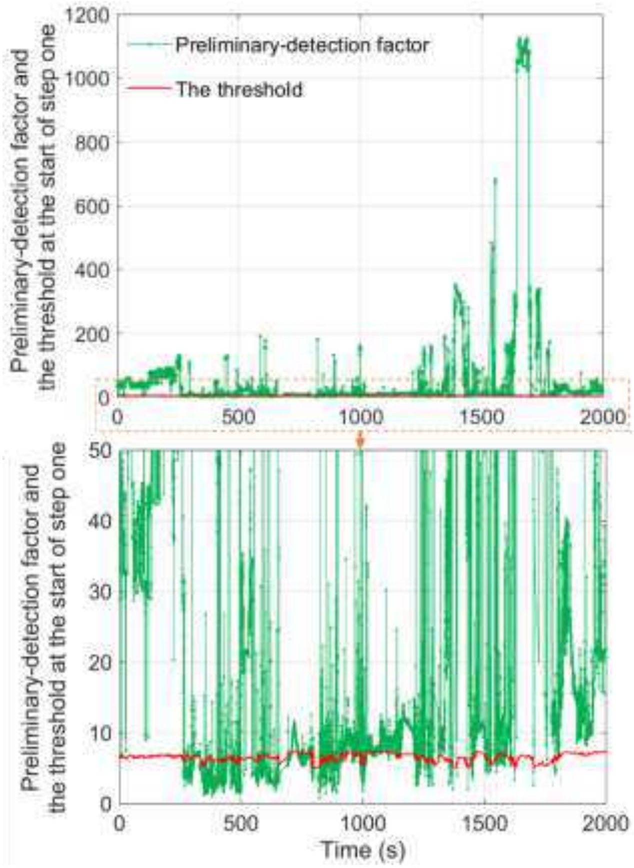

Fig. 5 Fault-detection factor and the threshold at the start of step one

After the preliminary FDE in step one, the fault-detection factor drops sharply as illustrated in Fig. 6. It is clear that the fault-detection factor is lower than the threshold most of the time, except in little epochs when the value of the fault-detection factor is slightly over the threshold. It should be noted that the threshold is also reduced with the reduction of the number of pseudoranges.

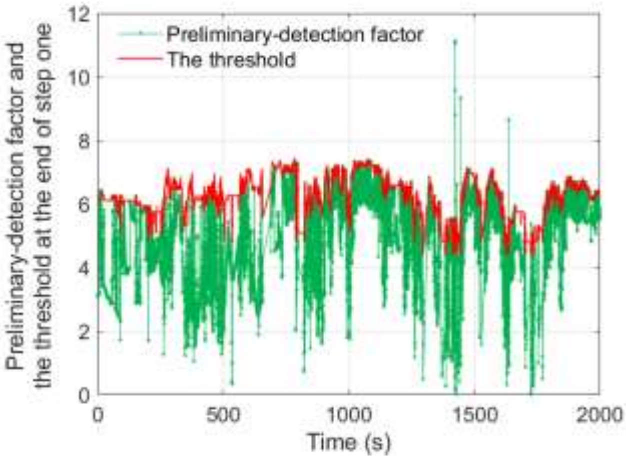

Fig. 6 Fault-detection factor and the threshold at the end of step one

The change in the number of visible BDS and GPS satellites is depicted in Fig. 7. It is common for more than one measurement to be identified as faulty by the preliminary FDE. In addition, the change of PDOP after step one is shown in Fig. 8. It is reasonable for the PDOP to get higher, because some measurements are excluded. However, excluding faulty measurements benefits the navigation algorithm.

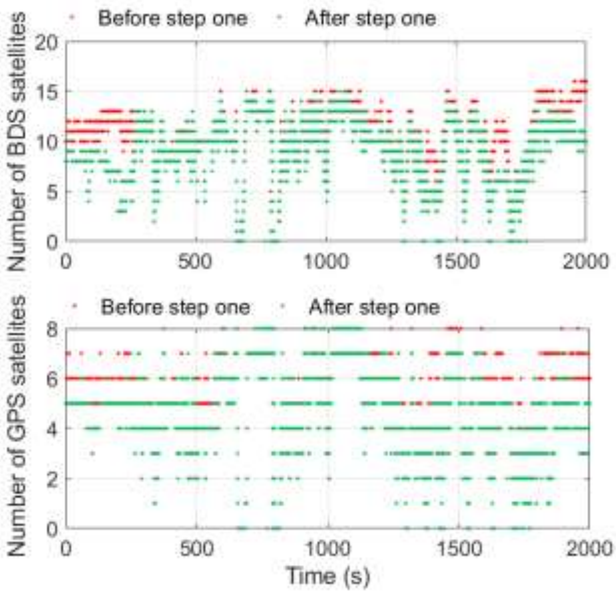

Fig. 7 Number of visible BDS and GPS satellites

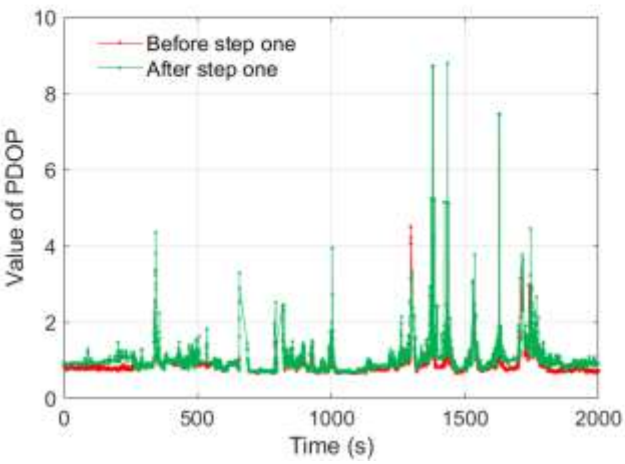

Fig. 8 Value of PDOP before and after step one

The preliminary fault exclusion is based on the single-fault-hypothesis subsets of the pseudorange. Fig. 9 shows the number of such subsets during the experiment. The maximum number of subsets is 175, and fewer than 100 subsets are needed in most fault-exclusion epochs. However, far more subsets are needed with ARAIM: for example, when 10 BDS satellites and 6 GPS satellites are visible, and just considering the possibility of fewer than 4 faulty measurements, $C_{16}^{1} + C_{16}^{2} + C_{16}^{3} = 696$ subsets should be included in calculations with ARAIM. It should be noted that the number of subsets increases rapidly when there are more visible satellites or more possible faulty measurements with ARAIM.

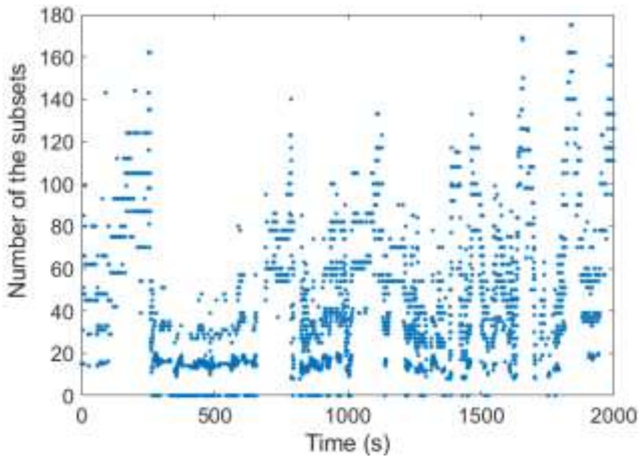

Fig. 9 Number of the single-fault-hypothesis subsets

After the preliminary FDE, a missed-detection check or false-alarm check is performed according to the value of the flag determined in step one. Fig. 10 depicts the missed-detection-check factor and the threshold during the experiment. It is clear that the value of the missed-detection-check factor is smaller than the predetermined threshold in a great number of epochs. There also are some epochs when the missed-detection-check factor exceeds the threshold.

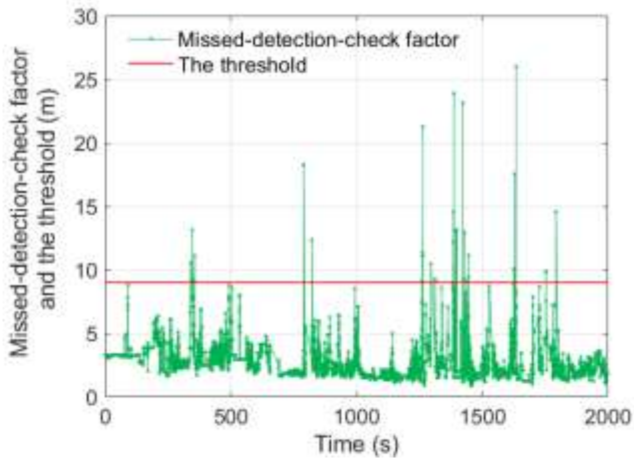

Fig. 10 The value of missed-detection-check factor and the threshold

Fig. 11 shows the value of the false-alarm-check factor and the threshold. The count of epochs when the false-alarm check was performed is less than that when missed-detection check was performed. The false-alarm-check factor is lower than the threshold in the major part of those epochs. As illustrated before, if the false-alarm-check factor is lower than the threshold, the solution of the remaining GNSS measurements is still used to update the GNSS/IMU integrated filter.

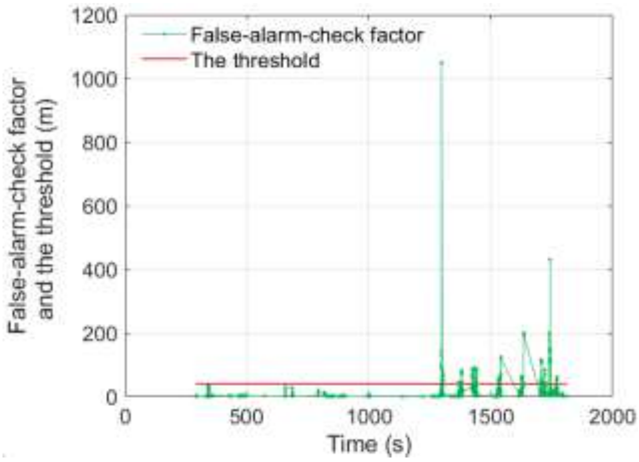

Fig. 11 The value of false-alarm-check factor and the threshold

In order to evaluate the improvement in performance of the proposed algorithm, (1) traditional EKF-based fusion algorithm and (2) EKF based fusion with LSR FDE are two candidate algorithms. The settings of EKF paramaters of the proposed algorithm and the two candidate algorithms are the same. The detailed steps of the algorithms are shown in Table 2.

Table 2 Summary of the algorithms

Candidate algorithm	Algorithm description
EKF	GNSS and IMU fusion is implemented in a loosely coupled mode with EKF. The measurement vector is based on the position and velocity solutions of GNSS measurements.
EKF with LSR FDE	Step 1: LSR FDE is implemented. Step 2: GNSS and IMU fusion is performed with EKF. The measurement vector is based on the position and velocity solution of normal GNSS measurements determined by LSR FDE.
Proposed Algorithm	Step 1: The FDE is performed via iterative consistency checking over the universal set and single-fault hypothesis subsets of the pseudoranges. Step 2: The preliminary FDE results are validated by missed-detection check and false-alarm check. Step 3: GNSS and IMU fusion is performed with EKF. The measurement vector is based on the position and velocity solution of normal GNSS measurements after step 2.

Positioning errors of the three algorithms in terms of the local-level coordinate system is shown in Fig. 12. The four parts enclosed by yellow dashed rectangles correspond to each of the four parts of the trajectory in Fig. 3. It can be seen that the positioning accuracy is improved greatly with the proposed algorithm in part 1, 3 and 4. Even though the positioning accuracy is also developed with LSR FDE, the extent to which the accuracy is improved is much smaller than that of the proposed algorithm. The total count of visible satellites is kept below 5 in the part-2 trajectory as Fig 6 shows. Thus, that is why the positioning accuracy is not improved with neither the proposed algorithm nor the EKF with LSR FDE.

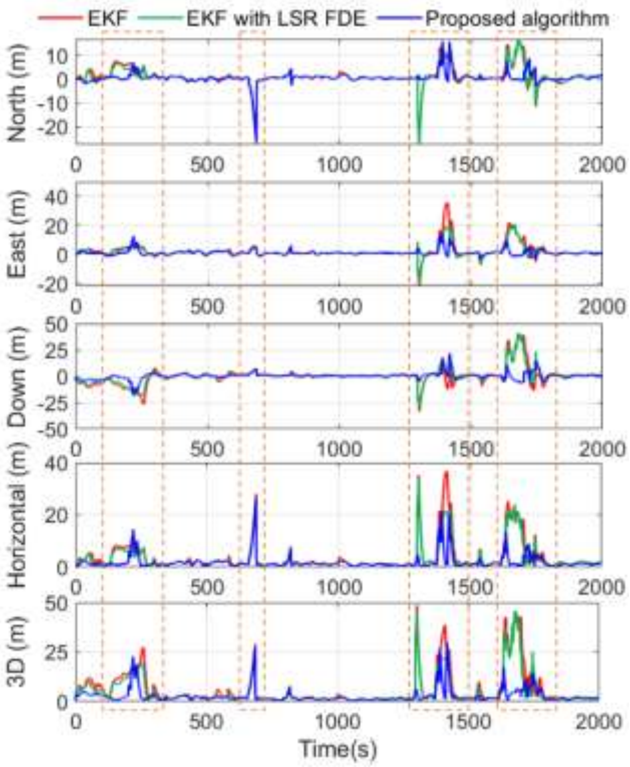

Fig. 12 Positioning errors in local-level coordinate system

The position root mean square error (RMSE) results are listed in Table 3, and the percentages of improvements in position accuracy are listed in Table 4. The horizontal and 3D position RMSE of the proposed algorithm are 3.296 m and 4.562 m respectively, corresponding to 52.2% and 56.9% improvements over the traditional EKF-based fusion algorithm, much higher than that of the EKF with LSR FDE.

Table 3 Position RMSE results comparison

Algorithm	Position RMSE (m)				
	North	East	Down	Horizontal	3D
EKF	4.157	5.504	8.014	6.898	10.574
EKF with LSR FDE	3.905	4.227	7.129	5.755	9.162
Proposed algorithm	2.430	2.227	3.154	3.296	4.562

Table 4 Position accuracy improvement compared to the traditional EKF-based fusion results

Algorithm	The improvement percentages of position accuracy (%)				
	North	East	Down	Horizontal	3D
EKF with LSR FDE	6.1	23.2	11.0	16.6	13.4
Proposed algorithm	41.5	59.5	60.6	52.2	56.9

The RMSE of velocity and altitude are listed in Table 5, and the accuracy improvement percentages are listed in Table 6. The integrated navigation system outputs notably more accurate velocities and altitudes with the proposed algorithm. The heading angle accuracy of the proposed algorithm is improved by 52.1% compared with the traditional EKF-based fusion. Even though there is a slight decrease of 0.3% in the accuracy of the pitch angle for the proposed algorithm, the magnitude of the pitch angle error is far lower than that of the heading angle error for all the three algorithms in the test. In addition, the proposed algorithm obtained a velocity accuracy development of over than 20%, which is much higher than that of the EKF with LSR FDE.

Table 5 Velocity and altitude RMSE results comparison

Algorithm	Velocity RMSE (m/s)			Altitude RMSE (Degree)		
	North	East	Down	Roll	Pitch	Heading
EKF	0.260	0.284	0.279	0.445	1.155	5.518
EKF with LSR FDE	0.220	0.267	0.249	0.450	1.161	4.526
Proposed algorithm	0.187	0.220	0.138	0.433	1.158	2.645

Table 6 Velocity and altitude accuracy improvement compared to the traditional EKF-based fusion results

Algorithm	The improvement percentages of velocity accuracy (%)			The improvements percentage of altitude accuracy (%)		
	North	East	Down	Roll	Pitch	Heading
EKF with LSR FDE	15.5	5.8	10.7	-1.2	-0.6	18.0
Proposed algorithm	28.1	22.5	50.4	2.6	-0.3	52.1

Conclusion

Ultimately, we developed a novel factor set based FDE scheme for integrated navigation of vehicles in urban environments. Simultaneous multiple faults can be detected and excluded efficiently with the proposed algorithm since far fewer subsets are included in the consistency check. Significantly, the missed-detection-check factor and the false-alarm-check factor are also designed to enhance the correctness and robustness of the FDE, and the performance of the proposed algorithm is validated by the real-life field test. The horizontal and 3D positioning accuracy of the proposed algorithm are 3.296 m and 4.562 m respectively in the deep-urban-environments field test. These results correspond to an over 50% improvement compared to the traditional EKF based GNSS/IMU loose fusion algorithm. Furthermore, the proposed algorithm resulted in a more than 20% improvement in velocity accuracy and a more than 50% improvement in heading accuracy.

Acknowledgement

The authors are grateful for the sponsorship of the National Natural Science Foundation of China (Grant No. 42174025, 41974033), the Natural Science Foundation of Jiangsu Province (Grant No. BK20211569), the University Grants Committee of Hong Kong under the scheme Research Impact Fund (Grant No. R5009-21), and Research Institute of Land and System, Hong Kong Polytechnic University.

Author Contributions

Conceptualization, H.C. and R.S.; Methodology, H.C. and R.S.; Data curation, H.C.; Software, H.C.; Formal analysis, R.S.; Supervision, R.S., Q.C. and L.Y.; Writing—original draft, H.C.; Writing—review & editing, H.C., R.S., Q.C and L.Y. All authors have read and agreed to the published version of the manuscript.

Competing interests

The authors declare that they have no competing interests as defined by Springer, or other interests that might be perceived to influence the results and/or discussion reported in this paper.

Data Availability

The datasets analyzed during the current study are available from the corresponding author on reasonable request.

References

Bhattacharyya S, Mute D (2020) Kalman sequential RAIM for reliable aircraft positioning with GPS and NavIC constellations. Sensors, 20(22): 6606. https://doi.org/10.3390/s20226606

Blanch J, Walter T, Enge P, Lee Y, Pervan B, Rippl M, Spletter A (2012) Advaced RAIM User Algorithm Description: Integrity Support Message Processing, Fault Detection, Exclusion, and Protection Level Calculation. In: Proceedings of the 25th International Technical Meeting of the Satellite Division of The Institute of Navigation (ION GNSS 2012). Pp. 2828-2849.

Blanch J, Walter T, Enge P (2013) Optimal positioning for advanced RAIM. J Inst Navig, 60(4): 279-289. https://doi.org/10.1002/navi.49

Blanch J, Walter T, Enge P (2015) Fast multiple fault exclusion with a large number of measurements. In: Proceedings of the 2015 International Technical Meeting of The Institute of Navigation. Pp. 696-701.

Chen Q, Zhang Q, Niu X (2020) Estimate the pitch and heading mounting ang les of the IMU for land vehicular GNSS/INS integrated system. IEEE Tra ns Intell Transp Syst, 22(10), 6503-6515. https://doi.org/10.1109/TITS.2020. 2993052

Cheng Q, Chen P, Sun R, Wang J, Mao Y, Ochieng WY (2021) A New Faulty GNSS Measurement Detection and Exclusion Algorithm for Urban Vehicle Positioning. Remote Sens, 13, 2117. https://doi.org/10.3390/rs13112117

Feng S, Ochieng WY, Walsh D, Ioannides R (2006) A measurement domain receiver autonomous integrity monitoring algorithm. GPS Solut, 10(2):85-96. https://doi.org/10.1007/s10291-005-0010-8

Feng S, Ochieng WY (2007) A Difference Test Method for Early Detection of Slowly Growing Errors in GNSS Positioning. J Navig, 60(3):427-442. https://doi.org/10.1017/S037346330700433X

Hwang DH, Oh SH, Lee SJ, Park C, Rizos C (2005) Design of a low-cost attitude determination GPS/INS integrated navigation system. GPS Solut, 9(4), 294-311. https://doi.org/10.1007/s10291-005-0135-9

Kaddour M, EI Najjar ME, Naja Z, Tmazirte NA, Moubayed N (2015) Fault detection and exclusion for GNSS measurements using observations projection on information space. In: 2015 Fifth International Conference on Digital Information and Communication Technology and its Applications (DICTAP). Pp. 198-203. https://doi.org/10.1109/DICTAP.2015.7113199

Lee YC (1986) Analysis of range and position comparison methods as a means to provide GPS integrity in the user receiver. In: Proceedings of the 42nd Annual Meeting of the Institute of Navigation. Pp. 1-4.

Li R, Zheng S, Wang E, Chen J, Dai L (2020) Advances in BeiDou Navigation Satellite System (BDS) and satellite navigation augmentation technologies. Satell Navig, 1(1): 1-23. https://doi.org/10.1186/s43020-020-00010-2

MacGougan G, Lachapelle G, Klukas R, Siu K, Garin L, Shewfelt J, Cox G (2002) Performance analysis of a stand-alone high-sensitivity receiver. GPS Solut, 6(3):179-195. https://doi.org/10.1007/s10291-002-0029-z

Parkinson BW, Axelrad P (1988) Autonomous GPS integrity monitoring using the pseudorange residual. J Inst Navig, 35(2):255-274. https://doi.org/10.1002/j.2161-4296.1988.tb00955.x

Sabatini R, Moore T, Ramasamy S (2017) Global navigation satellite systems performance analysis and augmentation strategies in aviation. Progress in Aerospace Sciences, 95(nov.), 45-98. https://doi.org/10.1016/j.paerosci.2017.10.002

Sturza MA (1988) Navigation system integrity monitoring using redundant measurements. J Inst Navig, 35(4):483-501. https://doi.org/10.1002/j.2161-4296.1988.tb00975.x

Sun D, Petovello MG, Cannon ME (2010) Use of a reduced IMU to aid a GPS receiver with adaptive tracking loops for land vehicle navigation. GPS Solut, 14(4), 319-329. https://doi.org/10.1007/s10291-009-0159-7

Sun R, Wang J, Cheng Q, Mao Y, Ochieng WY (2021) A new IMU-aided multiple GNSS fault detection and exclusion algorithm for integrated navigation in urban environments. GPS Solut, 25(4): 1-17. https://doi.org/10.1007/s10291-021-01181-4

Sun R, Zhang Z, Cheng Q, Ochieng WY (2022) Pseudorange error prediction for adaptive tightly coupled GNSS/IMU navigation in urban areas. GPS Solut, 26(1): 1-13. https://doi.org/10.1007/s10291-021-01213-z

Wang J, Ober PB (2009) On the availability of fault detection and exclusion in GNSS receiver autonomous integrity monitoring. J Navig, 62(2), 251-261. https://doi.org/10.1017/S0373463308005158

Wang S, Zhan X, Zhai Y, Liu B (2020) Fault detection and exclusion for tightly coupled GNSS/INS system considering fault in state prediction. Sensors, 20(3), 590. https://doi.org/10.3390/s20030590

Zabalegui P, De Miguel G, Pérez A, Mendizabal J, Goya J, Adin I (2020) A review of the evolution of the integrity methods applied in GNSS. IEEE Access, 8: 45813-

45824. https://doi.org/10.1109/ACCESS.2020.2977455

Zhu B, Meng F (2017) Integrity monitoring with MAIME upon integrated GNSS/SINS for SGEs. In: 2017 3rd IEEE International Conference on Computer and Communications (ICCC). Pp.1595-1600. https://doi.org/10.1109/CompComm.2017.8322809

Zhu N, Marais J, Bétaille D, Berbineau M (2018) GNSS position integrity in urban environments: A review of literature. IEEE Transactions on Intelligent Transportation Systems, 19(9): 2762-2778. https://doi.org/10.1109/TITS.2017.2766768

Author Biographies

Hanzhi Chen received a B.S. degree in traffic engineering from Chang'an University of China, Xi'an, Shaanxi, China, in 2020. He is currently pursuing a doctor's degree in transportation engineering at Nanjing University of Aeronautics and Astronautics. His research interest includes multisensor fusion algorithms for intelligent transportation system applications.

Rui Sun is currently an associate professor in the College of Civil Aviation, Nanjing University of Aeronautics and Astronautics, Nanjing, Jiangsu Province, China. She has a Ph.D. in Intelligent Transport Systems (ITS) from the Imperial College Engineering Geomatics Group (ICEGG) at Imperial College London and holds a M.Sc. in Satellite Positioning Technology from the University of Nottingham. Her research interests include seamless positioning and navigation in challenging environments. She was elected as a Fellow of the Royal Institute of Navigation (FRIN) and Editorial Advisory Board (EAB) member of the Journal of Navigation in 2021.

Qi Cheng received Bachelor's and Master's degrees in Transportation Engineering from NUAA, Nanjing, Jiangsu Province, China in 2017 and 2021 and is currently a PhD student in the Department of Land Surveying and Geo-Information at PolyU. His research interest is GNSS NLOS detection algorithms for Intelligent Transport System (ITS) applications